HHS Public Access

Author manuscript

Mol Cancer Res. Author manuscript; available in PMC 2019 February 01.

Published in final edited form as:

Mol Cancer Res. 2018 February ; 16(2): 256–268. doi:10.1158/1541-7786.MCR-17-0304.

Reprograming of Glucose Metabolism by Zerumbone Suppresses Hepatocarcinogenesis

Nissar Ahmad Wani[1,5], **Bo Zhang**[2], **Kun-yu Teng**[3,5], **Juan M. Barajas**[3,5], **Tasneem Motiwala**[4], **Peng Hu**[3,5], **Lianbo Yu**[4], **Rafael Brüschweiler**[2,6,7], **Kalpana Ghoshal**[3,5], and **Samson T. Jacob**[1,5,*]

[1]Department of Cancer Biology and Genetics, The Ohio State University, Columbus, OH

[2]Department of Chemistry & Biochemistry, The Ohio State University, Columbus, OH

[3]Department of Pathology, The Ohio State University, Columbus, OH

[4]Department of Biomedical Informatics, The Ohio State University, Columbus, OH

[5]Comprehensive Cancer Center, The Ohio State University, Columbus, OH

[6]Department of Biological Chemistry and Pharmacology, The Ohio State University, Columbus, OH

[7]Campus Chemical Instrument Center (CCIC) NMR, The Ohio State University, Columbus, OH

Abstract

Hepatocellular carcinoma (HCC) is the most prevalent and highly aggressive liver malignancy with limited therapeutic options. Here, the therapeutic potential of zerumbone, a sesquiterpene derived from the ginger plant *Zingiber zerumbet*, against HCC was explored. Zerumbone inhibited proliferation and clonogenic survival of HCC cells in a dose-dependent manner by arresting cell at the G2/M phase, and inducing apoptosis. To elucidate the underlying molecular mechanisms, a phosphokinase array was performed that showed significant inhibition of the PI3K/AKT/mTOR and STAT3 signaling pathways in zerumbone treated HCC cells. Gene expression profiling using microarray and analysis of microarray data using Gene Set Enrichment Analysis (GSEA) and Ingenuity Pathway Analysis (IPA) revealed that zerumbone treatment resulted in significant deregulation of genes regulating apoptotic, cell cycle and metabolism. Indeed, tracing glucose metabolic pathways by growing HCC cells with $^{13}C_6$-glucose and measuring extracellular and intracellular metabolites by 2D nuclear magnetic resonance (NMR) spectroscopy showed a reduction in glucose consumption and reduced lactate production, suggesting glycolytic inhibition. Additionally, zerumbone impeded shunting of glucose-6-phosphate through the pentose phosphate pathway, thereby forcing tumor cells to undergo cell cycle arrest and apoptosis. Importantly, zerumbone treatment suppressed subcutaneous and orthotopic growth and lung metastasis of HCC xenografts in immune-compromised mice. In conclusion, these findings reveal a novel and

*Co-corresponding authors: Samson T. Jacob: 420 W 12th Avenue, Columbus Ohio 43210, Ph: (614) 688-5494, samson.jacob@osumc.edu or Kalpana Ghoshal: 420 W 12th Avenue, Columbus Ohio 43210, Ph: 614-292-8865, kalpana.ghoshal@osumc.edu.

Conflict of interest: No potential conflicts

potentially effective therapeutic strategy for HCC using a natural product that targets cancer cell metabolism.

Keywords

HCC; Warburg effect; metabolic therapy; cell cycle; apoptosis

Introduction

Hepatocellular carcinoma (HCC) is the most prevalent primary liver cancer and usually develops in the presence of specific clinical manifestations such as cirrhosis, chronic inflammatory conditions resulting from hepatitis B virus (HBV) or hepatitis C virus (HCV) infections, alcoholic and non-alcoholic steatohepatitis, and aflatoxin-mediated toxicity (1, 2). Due to limited treatment options, HCC is the second most common cause for cancer-related deaths worldwide. The prognosis for HCC patients is poor, with less than 30% of the patients qualifying for curative treatments such as tumor resection or liver transplantation. Sorafenib is the only approved targeted therapy for advanced HCC, but it prolongs patient survival only marginally (3). It is evident that there is an urgent need to identify therapeutic strategies to treat this deadly disease.

A central hallmark of cancer cells is the reprogramming of cellular metabolism to meet the bioenergetics and biosynthetic demands of malignant growth (3–5). Thus, there is abundant interest in developing therapies to selectively target these aberrant metabolic phenotypes (3–5). Multiple lines of evidence presented here identify zerumbone, a dietary compound derived from a ginger plant, as an inhibitor of oncogenic cues that promote liver tumorigenesis. Zerumbone is known to exhibit anti-proliferative and anti-inflammatory activities through the modulation of NF- B activity (6, 7). Zerumbone was also shown to have hepatoprotective properties in ethanol-induced liver injury in male Sprague Dawley rats, where zerumbone pretreatment extensively reduced fatty liver development in these rats (8). Importantly, zerumbone exhibits minimal effects on normal cells (6, 7).

The cytotoxic effect of zerumbone on cancer cells appears most likely due to its versatile α, β-unsaturated carbonyl group, which plays an important role in its interaction with the cellular proteins. This carbonyl group effectively removes intracellular glutathione (GSH) through the formation of Michael adducts causing elevation of its intracellular redox potential (9). The markedly reduced effect of this compound on the proliferation of normal cells is probably caused by the difference in the average intracellular redox potential between normal cells and cancerous cells (7). Although zerumbone exhibits strong anti-proliferative, anti-metastatic and pro-apoptotic properties against some cancer cells, its precise molecular mechanism of action has not been fully elucidated. Here, we investigated the anti-HCC efficacy of zerumbone *in vitro* and *in vivo* and elucidated the underlying mechanism using unbiased approaches, focusing on its role in reprograming metabolism in HCC.

Materials and Methods

Reagents and antibodies

Dulbecco's Modified Eagle's Medium (DMEM), Minimum Essential Medium Eagle (MEM), FBS, Zerumbone were purchased from Sigma-Aldrich (St. Louise, MO). Cell Titer GLO kit purchased from Promega Life Sciences (Madison, WI). The catalogue numbers and sources of all antibodies are provided in Supplementary Table S1.

Cell lines and culture

Human HCC cell lines (HepG2, Hep3B, Sk-Hep-1, SNU-182, SNU-449) were purchased from the ATCC. Huh-7 and MHCC-LM3 cells were provided by Drs. James Taylor (Fox Chase Center, PA, USA) and Dr. Hangxiang Wang (The First Affiliated Hospital, School of Medicine, Zhejiang University, Hangzhou, China), respectively. Mouse Hepa1 cells were provided by Dr. Gretchen Darlington at Baylor College of Medicine. All cells were maintained in Minimum Essential Media supplemented with L-glutamine (2 mM), 10% FBS, sodium pyruvate (0.11 g/L) and penicillin/streptomycin (100 U/mL) at 37°C with 5% CO_2. THLE2 cells obtained from ATCC was cultured in William E medium supplemented with EGF (5 ng/mL), phospho-ethanolamine (70 ng/mL), 1X GlutaMax, 10% FBS, sodium pyruvate (0.11 g/L) and penicillin/streptomycin (100 U/mL) at 37°C with 5% CO_2.

In vitro growth inhibition assay

HCC cells were seeded into 96-well plates (3×10^3 cells/well) and after 24 hour were treated with various concentrations of zerumbone dissolved in DMSO (final concentrations <0.1% in the medium). Cells. After 48 hours of treatment, viability of cells was assessed using CellTiter-GLO kit that measures ATP levels in cell extracts.

Clonogenic survival assay

For the clonogenic survival assay, HCC cells (500) were plated in each well of 6-well plate in 2.5 mL of culture medium. After 48 hours, cells were treated with zerumbone at different concentrations; fresh medium with zerumbone was replaced every 72 hour. After 15 days, colonies were fixed in 4% formaldehyde and stained with 0.5% crystal violet (10).

Cell-cycle analysis

Cells at distinct phases of the cycle were distinguished by staining DNA with propidium iodide (PI) and measured by flow cytometry. HCC cells (1×10^6 cells/mL) were treated with 50 μM of zerumbone and incubated for 24 and 48 hours. Cells were then collected, washed with ice-cold PBS and fixed in ice-cold 70% ethanol and stored at −20°C overnight. The cells were centrifuged, washed with phosphate-buffered saline (PBS) and resuspended in 0.4 mL of PBS. To a 0.5 mL cell suspension, 50 μL of RNase A (1 mg/mL in PBS) was added and incubated for 30 min at 37°C, followed by the addition of 50 μL of PI (500 μg/mL in PBS) with gentle mixing and incubation in the dark at room temperature for 15 min and stored at 4°C until analyzed by flow cytometry using a LSRII flow cytometer (BD Biosciences, CA). The data were acquired and distribution of cells in G1-, S- and G2–M phases was determined using ModFit LT 3.2 (Verity Software House) program.

Apoptosis assay

HCC cells were treated with zerumbone for 24 and 48 hours. Apoptosis was determined with the Annexin V-PE/7-AAD apoptosis kit (BD Biosciences, CA) as per the manufacturer's instructions. Briefly, cells were trypsinized, washed twice with ice-cold PBS and the pellet was resuspended in 100 μL binding buffer (50 mM HEPES/NaOH, pH 7.4, 700 mM NaCl, 12.5 mM $CaCl_2$) containing 5 μL each of Annexin V-PE and 7-AAD. After incubation for 15 minutes at room temperature in a light-protected area, another 400 μL of binding buffer was added, and the specimens were quantified by flow cytometry. The early apoptotic (Annexin V-PE-positive) and late apoptotic (Annexin V-PE-positive, 7AAD-positive) cells were quantified as apoptotic cells.

Human phospho-protein array

Huh-7 and MHCC-LM3 cells were treated with zerumbone (50 μM) for 24 hours and cell lysates were subjected to phosphoprotein analysis using The PathScan RTK Signaling Antibody Array Kit (BD Bioscience) following manufacturer’s protocol to quantify phosphorylation levels of 43 proteins phosphorylated at tyrosine/serine/threonine residues.

Western blot analysis

Proteins extracted from cells or tissues were immunoblotted with different antibodies following published protocol (10). Briefly, cells treated with zerumbone or DMSO (vehicle) were processed for immunoblotting. Lysate proteins were resolved by sodium dodecyl sulfate-polyacrylamide gel electrophoresis, transferred onto Nitrocellulose membrane and immunoblotting was performed. After blocking with blocking buffer (LI-COR, Lincoln, NE, USA), the membrane was incubated with primary antibodies overnight at 4°C. Following incubation with appropriate secondary antibody (IRD-680 or IRD-800), the immunoreactive bands were visualized using LI-COR-Odyssey infrared scanner (LI-COR). The blots were re-probed with anti-actin or GAPDH antibody to correct for differences in protein loading. Protein concentrations were estimated using a Bio-Rad protein assay kit with bovine serum albumin as standards.

Microarray analysis of HCC cells

Total RNA from the MHCC-LM3 cells was isolated using TRIzol (Invitrogen) and purified using RNeasy Mini columns (QIAGEN), and the integrity and quantity of the RNA were assessed using an Agilent Bioanalyzer and Nanodrop RNA 6000, respectively. Total RNA was labeled using the Affymetrix Whole Transcript Sense Target Labeling kit and hybridized to the Affymetrix human Exon 2.0 ST array following the manufacturer’s protocol at the Microarray Shared Resource Facility at The Ohio State University Comprehensive Cancer Center. To identify biological concepts associated with zerumbone treatment, we performed Gene Set Enrichment Analysis (GSEA) on the microarray data. Differentially expressed genes were uploaded into GSEA software ($Log_2FC > 2$, p-value < 0.05). The biological processes, cellular components, molecular functions, and gene networks, were obtained by uploading the same subset of data to be analyzed using Ingenuity® Pathway Analysis tools (Ingenuity Systems Inc., Mountain View, CA).

Ingenuity pathway analysis

The IPA application (http://www.ingenuity.com/products/IPA/Free-Trial-Software.html) was used to identify gene networks that were overrepresented among the genes that exhibited ≥ 2 fold up- or down-regulation with a p-value ≤0.0001 in zerumbone treated MHCC-LM3 cells. A significance score of ≥3 indicates that there is a less than 1 in 1000 chance that the highlighted genes were assembled into a network due to a random chance.

Reverse transcription - quantitative polymerase chain reaction (qRT-PCR)

For gene expression analysis, DNase I treated total RNA was reverse-transcribed into complementary DNA (cDNA) using a high-capacity cDNA reverse transcription kit (Applied Biosystems) and real-time PCR was performed using SYBR Green chemistry. The expression was normalized to that of GAPDH or β-actin. All real-time reactions, including controls without cDNA, were run in triplicate in a thermocycler. Relative expression was calculated using the comparative CT method. PCR primer sequences are provided in the Supplementary materials (Supplementary Table S2).

NMR-based metabolomics analysis

Huh7, HepG2 and MHCC-LM3 cells (around 1.5×10^7 cells each) were seeded in triplicate in 100 mm plates, grown to 70–80% confluence and changed to media containing 5 mM U-$^{13}C_6$-glucose (Cambridge Isotope Laboratories, Inc., Andover, MA), 3% dialysed FBS and treated with zerumbone (50 μM) or DMSO (0.1%) for 24 hours. An aliquot (0.2 mL) of the culturing media at 0, 12, 24 and 36 hours were collected and hydrophilic metabolites were extracted, lyophilized and dissolved in 50 mM phosphate buffer (pH 7.4). Metabolites were also extracted from cells after 24, 36 and 48 hours and were subjected to NMR analysis. 2D ^{13}C-edited ^{1}H-^{1}H TOCSY spectra were collected at 298 K on a Bruker 700 MHz AVANCE III spectrometer equipped with a TXO cryoprobe (11). The peak intensities of ^{13}C labeled glucose and lactic acid were used to measure their relative changes at different time points.

The cell lysate samples were dissolved in D_2O and 0.1 mM DSS was added as an internal chemical shift standard. 2D ^{13}C-^{1}H HSQC spectra, 2D ^{1}H-^{1}H TOCSY spectra and 2D ^{13}C-^{1}H HSQC-TOCSY spectra were collected at 298 K on a Bruker 850 MHz ACANCE III spectrometer with a TCI cryoprobe. 2D HSQC cross-peak positions were extracted (peak picking) and subsequently queried against the COLMARm NMR metabolomics database and validated using the two TOCSY experiments (12). Metabolite concentrations were quantified based on HSQC cross-peak intensities normalized by the average intensity of all identified metabolites. For each cell line, the maximal intensity of each cross-peak across the whole dataset was set to 1 and the peak intensities in the other data sets were scaled relative to this peak. For metabolites with multiple cross-peaks, average peak intensities were used instead.

Antitumor efficacy of zerumbone *in vivo*

NSG mice were purchased from Target Validation Shared Resource (TVSR) core facility at The Ohio State University Comprehensive Cancer Center and were housed in sterile facility under a 12/12-hour light/dark cycle. All the animal studies have been conducted in

accordance with an Institutional Animal Care and Use Committee (IACUC). For ectopic model, Huh7 (5×10^6/100 μL) were injected in the right flank of NSG mice. On 14th day mice were randomized into 2 groups (6 mice/group) and injected intraperitoneally with Hydroxypropyl beta-Cyclodextrin (HPBCD), or zerumbone (20 mg/kg/day). Tumor volumes based on caliper measurements were calculated by the ellipsoidal formula (1/2(length × width^2)). After 21 days of treatment, mice were euthanized and tumor tissues were collected, photographed and weighed. An orthotopic xenograft model of liver cancer was established. Briefly, subcutaneous tumors developed by MHCC-LM3 cells injected in the flanks of NSG-mice were harvested and necrotic tissues were removed carefully. A piece (1 mm^3) of the tumor tissue was transplanted into the largest liver lobe of each NSG mouse. The tumor-bearing mice were randomized into 2 groups (4 mice/group) and injected intraperitonally with vehicle HPBCD, or zerumbone (20 mg/kg/day). After 3 weeks, tumor tissues were collected, photographed and weighed. Lungs were removed and fixed in Bouin's solution and FFP sections were subjected to histology.

Histology and immunohistochemical analyses

For histology, tissues were fixed in 4% paraformadehyde and embedded in paraffin. For immuno-histochemical analysis, the slides were dewaxed and subjected to antigen retrieval at 95°C for 30 minutes, followed by incubation with the antibodies and color development by the DAB method (13).

Statistical analysis

For *in vivo* mice tumor study, we used linear mixed model for repeated measures and t-test for testing difference at each time point. For cell line data, statistical significance of differences between groups was analyzed by two-sample unpaired Student's t-test. All qRT-PCR (assayed in triplicate) and Western blotting experiments were repeated twice, and reproducible results were obtained. Single, double and triple asterisks denote $p \leq 0.05$, ≤ 0.01 and ≤ 0.001, respectively.

Results

Zerumbone inhibits tumorigenic potential of HCC cells by inhibiting cell cycle progression and promoting apoptosis

To investigate the anti-tumorigenic functions of zerumbone on HCC cells, we initially determined its IC_{50} in different HCC cell lines. Its Anti-proliferative activity was evident after 48 hours; IC_{50}s ranging from 60 μM for MHCC-LM3 cells to 90 μM for Hep3B cells (Fig. 1A). As expected, growth inhibitory effect of this dietary compound was more pronounced after 72 hours as demonstrated by IC_{50} of 14 μM for HepG2 cells to 31 μM for Huh7 cells (Supplementary Fig. S1). We found that zerumbone also inhibited proliferation of transformed THLE-2 cells after 72hrs, albeit less effectively than in HCC cells (IC_{50}, 38 μM).

We also analyzed clonogenic survival, an indicator of long-term survival of tumor cells and a predictor of the long-term anti-tumorigenic effects of drugs (10). Zerumbone inhibited colony numbers of HepG2, Hep3B and Huh7 cells as well as highly metastatic MHCC-LM3

cells in a dose dependent manner at sub-micromolar range (Fig. 1B–C; Supplementary Fig. S2). Compared to well-developed colonies formed in control cells, both number and size of colonies formed were significantly reduced upon zerumbone exposure. We could not do this assay in THLE-2 cells since they form colonies from single cells.

To elucidate the underlying mechanism, we initially analyzed cell cycle profile of HCC cell lines treated with zerumbone (50 μM), a concentration less than its IC_{50} values measured at 48h (Fig. 1A). Zerumbone treatment arrested cells at G2/M phase, as demonstrated by the accumulation of cells at S and G2/M phases with a concomitant decrease in the population of cells at G1 phase in drug treated cells compared to vehicle treated controls (Fig. 1D, E; Supplementary Fig. S2). Further, this cell cycle arrest was time dependent, with greater accumulation of cells in S and G2/M phases after 48 hours compared to 24 hours, suggesting that zerumbone-mediated alterations in checkpoint might promote apoptosis of damaged cells instead of their progression through cell cycle. Indeed, flow cytometric analysis of Annexin V/7-AAD stained HCC cells showed 18–20% increase in apoptotic cells after 24 hours exposure to zerumbone (50 μM), which increased further after 48 hours (Fig. 1F; Supplementary Fig. S2) Taken together, these results suggest that zerumbone-induced cell cycle arrest and apoptosis play a key role in its anti-tumorigenic effect.

Zerumbone (ZER) inhibits expression of genes regulated by PI3K/AKT/mTOR and STAT3 signaling pathways

To elucidate the molecular mechanisms underlying zerumbone-mediated HCC cell death, we analyzed gene expression profile by microarray of highly metastatic MHCC-LM3 cells treated with zerumbone (50 μM) for 24 hours. Zerumbone exposure resulted in significant upregulation (>2 fold) of 1515 genes and downregulation (>2 fold) of 2441 genes compared to vehicle controls (Fig. 2A). Ingenuity pathway analysis (IPA) of the microarray data showed that the zerumbone-deregulated genes were mostly associated with pathways involved in cancer development, specifically cell cycle regulation, and PI3K/AKT and STAT3 signaling (Fig. 2B and Supplementary Table S3). Gene Set Enrichment Analysis (GSEA) confirmed that genes regulated by these signaling pathways were significantly enriched in the zerumbone-treated MHCC-LM3 cells (Fig. 2C, D; Supplementary Fig. S3). These results suggest that deregulation in these pathways might be a major contributing factor in the pathogenesis of HCC, and by virtue of its ability to inhibit these pathways zerumbone holds a great potential as a therapeutic agent for HCC.

Next, we queried whether PI3K/AKT/mTOR and STAT3 pathways are indeed targets of zerumbone. To this end, we profiled phosphoprotein array with lysates of MHCC-LM3 and Huh-7 cells treated with zerumbone (50 μM) for 24 hours. The results demonstrated that zerumbone inhibited phosphorylation of ERK (T202/Y204), p53 (S392, S15 & S46), AKT (S473 & T308), mTOR (S2448), CREB (S133), STAT3 (Y705), CHK-2 (T68), and WNK1 (T60), as well as enhanced phosphorylation of c-JUN (S63), LCK (Y394), and RSK1–3 in these cells compared to the vehicle control (Fig. 3A, B; Supplementary Fig. S4). Validation of these results by immunoblotting confirmed that zerumbone indeed reduced phosphorylation of AKT (S473), mTOR (S2448) and STAT3 (Y705) in Huh7, MHCC-LM3 and HepG2 cells (Fig. 3C, D; Supplementary Fig. S4). Notably, total Akt level was also

reduced by 40 to 60% upon zerumbone treatment (Supplementary Fig. S4). These results demonstrated indeed PI3K/AKT/mTOR and STAT3 signaling pathways were inhibited by zerumbone that might caused altered expression of their target genes as observed in gene expression profiling (Fig. 2).

Zerumbone modulates expression of genes involved in cell cycle and apoptosis

To elucidate the mechanisms by which zerumbone treatment impacts cell cycle progression, we focused on the pathway analysis that showed association of a large number of zerumbone-deregulated genes with cell cycle progression (Fig. 4A, B). Among these, downregulation of several genes such as *CCNB2, SKP2, CCND1, HIPK2, CCND1*, *PLK1*, *CDC25B* and upregulation of *GADD45A* and *CDKN1A* in zerumbone-treated HCC cells were confirmed by qRT-PCR (Fig. 4C). Since zerumbone treatment of HCC cells induced cell cycle arrest at G2/M phase (Fig. 1D, E; Supplementary Fig. S2), and significant alteration in cell cycle regulating genes (Fig. 4A–C), we explored the possibility that the expressions of proteins involved in G2 phase regulation may also be modulated by zerumbone. Indeed, Cyclin A2 and CDK1 levels were significantly reduced in Huh7 and HepG2 cells treated with the drug for 24 hours, which was more pronounced after 48 hours (Fig. 4 D, E; Supplementary Fig. S5). These data indicate that the cell cycle arrest at G2/M phase is responsible for growth inhibition of HCC cells by zerumbone.

Next, we performed in-depth analysis of deregulated genes in zerumbone-treated MHCC-LM3 cells using transcriptome analysis. This study showed that 70% of the genes associated with apoptosis were upregulated whereas 30% were downregulated (Fig. 5A, B). qRT-PCR analysis confirmed significant increase in the expression of pro-apoptotic molecules such as *DIABLO, CASP3, BNIP3L, DEED, PMAIP1* and decrease in the expression of anti-apoptotic molecules such as ERCC2 and *HELLS* in MHCC-LM3, Huh7 and HepG2 cells treated with zerumbone (Fig. 5C). Upregulation of apoptotic pathway in zerumbone treated cells was associated with activation of apoptotic proteins as demonstrated by increased PARP cleavage together with decrease in procaspase 7 and procaspase 9 (Fig. 5 D–F; Supplementary Fig. S5). Interestingly, the anti-apoptotic signal (BCL-2 expression) was also reduced in zerumbone treated Huh-7 and MHCC-LM3 cells (Fig. 5 D–F). These data tend to conclude that zerumbone promotes apoptosis in HCC cells by activating pro-apoptotic and inhibiting anti-apoptotic gene expression signature.

Zerumbone reprograms glucose metabolism in HCC cells

There is a growing appreciation that metabolic signals are integrated and coupled to cell cycle progression (14, 15) and that activation of AKT and mTOR signaling regulates cancer cell metabolism (3, 16). We hypothesized that zerumbone might regulate energy metabolism in HCC cells by modulating these signaling pathways that resulted in cell cycle arrest. To explore the key zerumbone-mediated metabolic alterations in these cells, we initially measured glucose consumption and lactate production in drug-treated HCC cells. For this purpose, Huh7 cells grown in glucose-free DMEM supplemented with 5 mM $^{13}C_6$-glucose were treated with zerumbone (50 μM) or vehicle (DMSO) followed by estimation of glucose and lactate levels in culture supernatants at different time points by NMR. The results showed significant suppression of $^{13}C_6$-glucose consumption and reduced ^{13}C-lactate

production in HCC cells after 24 hours of zerumbone treatment, a trend that continued over the next 12 hours (Fig. 6A). Next, we determined whether these changes were due to alterations in cellular metabolism, by performing intracellular metabolomics in zerumbone-treated Huh-7, MHCC-LM3 and HepG2 cells using 2D ^{13}C-^{1}H NMR (Fig. 6B; Supplementary Fig. S6). We observed accumulation of intracellular $^{13}C_6$-glucose and reduction in the levels of several glycolytic intermediates such as glycerol-3-phosphate and 3-phosphoglycerate in zerumbone treated HCC cells (Fig. 6B, C; Supplementary Fig. S7 and S8). These results suggest that the intracellular glucose metabolism through glycolysis was curtailed by zerumbone. Reduced lactate-to-pyruvate ratios indicate that the conversion of pyruvate to lactate was impeded in drug-treated Huh7 and HepG2 cells compared to DMSO controls (Fig. 6C; Supplementary Fig. S7 and S8). The lack of detection of pyruvate in MHCC-LM3 cells (Supplementary Fig. S7) suggests its rapid conversion to lactate or entry into TCA cycle.

It is noteworthy that glycolytic blockade, in particular at the conversion of glucose-6-phosphate (G6P) to fructose-6-phosphate (F6P) step, might increase shunting of glucose-6-phosphate (G6P) through pentose phosphate pathway (PPP) to produce energy and biomass ([3]). We, therefore, quantified PPP intermediates in HCC cells from the 2D ^{13}C-^{1}H HSQC NMR data. Among these, ribose-5-phosphate levels were reduced in Huh7 and HepG2 cells but were increased in MHCC-LM3 cells upon zerumbone treatment (Fig. 6D; Supplementary Fig. S7). If glycolysis is blocked, G6P can be converted to UDP-galactose whereas F6P can be diverted to generate glycolipids and glycerol. Indeed, zerumbone exposure elevated galactose-1-P and UDP-galactose (Fig. 6E; Supplementary Fig. S7 and S8) as well as acetyl-glucosamine, glucosamine and UDP-N-acetyl glucosamine levels (Fig. 6E; Supplementary Fig. 7 and S8) in HCC cells.

Since we observed diminished pyruvate to lactate conversion in zerumbone treated cells (Fig. 6C; Supplementary Fig. S7), the accumulation of pyruvate might lead to its conversion to acetyl-CoA and thereby, its entry into TCA cycle (Fig. 6F; Supplementary Fig. 7 and S8)). This increase in citrate probably led to its conversion to glutamate and glutamine via α-ketoglutarate (2-KG) in zerumbone treated cells (Fig. 6B). Collectively, these results suggest that the altered glucose metabolism could play a causal role in the anti-proliferative function of zerumbone.

Zerumbone regulates genes involved in glycolysis and pentose phosphate pathway

Pathway analysis of microarray data revealed deregulation of glycolysis and PPP genes. We confirmed deregulation of selected genes of these pathways by qRT-PCR in Huh7, MHCC-LM3 and HepG2 cells (Supplementary Fig. S9). Interestingly, the expression of several enzymes regulating glycolysis, namely glucose-6-phosphate isomerase (GPI), phosphofructokinase-1 also called phosphofructokinase M (PFKM), phosphoglycerate mutase (PGM) and lactate dehydrogenase (LDH), were reduced in zerumbone treated HCC cells compared to DMSO controls (Supplementary Fig. S9). Moreover, the expressions of genes regulating PPP e.g. glucose-6-phosphate dehydrogenase (G6PDH), ribulose-5-phosphate isomerase (RPIA), ribulose-5-phosphate-3-epimerase (RPE), trans-ketolase (TKT) and transaldolase-1 (TALDO1) were also suppressed in drug-treated HCC cells

(Supplementary Fig. S9). These results suggest that zerumbone treatment inhibited expression of key enzymes regulating glycolysis and PPP in HCC cells to inhibit their proliferation.

Zerumbone (ZER) retards HCC growth and metastasis *in vivo*

To confirm that the anti-tumorigenic effects of zerumbone observed *in vitro* can be replicated *in vivo*, we used a subcutaneous xenograft model established by injecting Huh7 cells into the flanks of NSG mice. We treated these mice with zerumbone (20 mg/kg) or vehicle when tumors reached palpable size and monitored tumor volume throughout treatment as well as tumor weight at the end of treatment. The results showed that zerumbone significantly blocked tumor growth (Fig. 7A) compared to the vehicle control. We also tested efficacy of zerumbone in NSG mice bearing orthotopically implanted tumor slices generated from subcutaneously developed tumors of MHCC-LM3 cells. This natural compound also inhibited orthotopic tumor growth of these cells (Fig. 7B; Supplementary Fig. S10), which correlated with reduced number (>50%) of Ki67-positive tumor cells and AFP expression (Fig. 7C, D). Notably, these highly aggressive cells formed metastatic nodules in the lung and zerumbone treatment significantly minimized their numbers (Fig. 7E, F). Cumulatively, these results demonstrate tumor suppressive potential of zerumbone *in vivo*.

Discussion

Hepatocellular carcinoma (HCC) is one of the deadliest cancers due to its complexities, reoccurrence after surgical resection, metastasis and heterogeneity (17). Deregulation of several signaling pathways in cancer cells leads to abnormal cellular bioenergetics, which provides cancer cells a distinct growth advantage either by supplying fuel for their proliferation or creating microenvironments conducive to cancer metastasis. Recently, there have been renewed interests in using natural compounds as chemo-preventive or therapeutic agents as many of these agents targeting metabolic pathways in cancer cells have therapeutic potential against HCC (18). We have been exploring the role of diets, DNA hypermethylation and microRNAs in inducing HCC in animal models (19–22), and are now extending this investigation to the use of natural compounds in blocking hepatocarcinogensis. The present study has clearly demonstrated that zerumbone treatment results in deregulation of molecular signals that modulate cell cycle and apoptosis, leading to impairment of HCC proliferation. In-depth analysis of the mechanisms responsible for reduced HCC tumorigenesis using microarray and phosphokinase array have shown a potential role of downregulation of PI3K/AKT/mTOR and STAT3 pathways by zerumbone in arresting liver tumorigenesis. Activation of these pathways has been associated with different malignancies including HCC (23, 24).

Cancer cells including HCCs are dependent on aerobic glycolysis, also called Warburg effect, to sustain growth (3, 4, 25). Reduced glucose consumption accompanied by reduced lactate production in HCC cells treated with zerumbone led us to hypothesize that zerumbone could inhibit HCC cell proliferation by modulating pathways associated with cell metabolism, and this altered metabolic profile may contribute to cell cycle arrest and

apoptosis. This key observation is consistent with the growing interest in coupling of metabolic signals to cell cycle progression (14, 15). Upregulation of glucose-6-phosphate isomerase (GPI) that converts glucose-6-phosphate (G6P) to fructose-6-phosphate (F6P) has been shown to stimulate cell motility, an important step in the metastatic process (26–28). This process is associated with poor survival of HCC patients (3). Thus, inhibition of GPI expression by zerumbone (Supplementary Fig. S11) will probably have an impact on the proliferation and metastatic potential of HCC cells.

Alteration in other pathways of glucose metabolism by zerumbone could also contribute to hampering growth and proliferation of HCC. Zerumbone is likely to impede glycolysis at multiple steps by suppressing the expression of Phosphofructokinase (PFKM), lactate dehydrogenase A (LDHA) and lactate dehydrogenase B (LDHB) that are upregulated in HCC (29). Prasannaet *et al.* have found that altered metabolic and signaling cues in response to glycolysis inhibition in cancer cells promote metabolic reprogramming to bypass or minimize glycolysis dependency (3). The reduced level of ribose-5-phosphate and increase in erythritol levels in zerumbone treated HCC cells were associated with diminished expression of glucose-6-phosphate dehydrogenase (G6PD) (Supplementary Fig. 9), the rate-limiting enzyme regulating pentose phosphate pathway (PPP). Indeed, blocking both glycolysis and PPP diverts G6P to produce higher levels of UDP-galactose as observed in HCC cells treated with zerumbone (Fig. 6, 7). These observations indicate that blocking glycolysis and shunting of G6P through PPP probably play a key role in suppressing HCC growth by zerumbone (Supplementary Fig. S11).

It is noteworthy that zerumbone-mediated reduction in Lactate dehydrogenase (LDHA and LDHB) expression leads to accumulation of pyruvate in the cells (Supplementary Fig. 9). Relatively high level of lactate in HCC is known to enhance cell motility, facilitate the breakdown of extracellular matrix to stimulate the migration of epithelial cancer cells, and promote cancer metastasis to distant organs (29). Zerumbone-induced inhibition of glycolysis can force pyruvate to enter TCA cycle thereby increasing TCA cycle intermediates as observed in HCC cells treated with zerumbone (Fig. 6). The zerumbone-induced increase in acetate and acetyl phosphate levels is consistent with the suppression of LDH and conversion of pyruvate to these metabolites in the treated cells (Fig. 6C; Supplementary Fig. S7 & S8). Dysregulated metabolism has also been linked to drug resistance. Thus, higher activity/expression of lactate dehydrogenase A (LDHA) contributes to paclitaxel/ trastuzumab resistance in breast cancer whereas increase in pyruvate dehydrogenase kinase 3 (PDK3) contributes to hypoxia-induced drug resistance in cervical and colon cancer (30). These observations suggest that coaxing tumors to utilize lactate or finding ways to reduce glycolysis and lactate production could retard liver tumorigenesis or prevent drug resistance, specifically resistance to sorafenib, the only FDA approved drug for advanced HCC.

There is ample evidence on the functional relationship between metabolic signals and cell cycle progression (14, 15). Early gene expression studies suggested that the expression of metabolic enzymes is synchronized with certain discrete phases of cell cycle progression. For instance, using *S. cerevisiae* as a model, it was shown that many mitochondrial enzymes required for glycolysis and oxidative phosphorylation were induced in early G1 phase (31).

It is likely that metabolic alterations at early stage might send signals to stop or slow down cellular growth. Moreover, it is well documented that cell cycle arrest at the G2-M phase could prevent damaged cells from undergoing mitosis, thus promoting apoptosis (32). The cell cycle arrest at S and G2/M phases corroborated with zerumbone-mediated inhibition of PPP required for DNA and RNA synthesis.

In conclusion, we have demonstrated that zerumbone prevents liver tumorigenesis in *vitro* and *in vivo* by regulating cancer cell metabolism thereby forcing cells to undergo cell cycle arrest and apoptosis (Supplementary Fig. S11). Based on the data presented in this study, it is conceivable that the dietary components like zerumbone may be excellent therapeutic options for treating HCC. Since the majority of hepatocellular carcinomas are diagnosed at late stages and most HCC patients at late stages are resistant to sorafenib, the only FDA-approved drug to treat advanced HCC, combination of sorafenib with zerumbone could be more effective in targeting advanced HCCs. Our *in vitro* and *in vivo* data indicate that targeting cancer cell metabolism may be an alternate and effective approach to suppress hepatocarcinogenesis.

Supplementary Material

Refer to Web version on PubMed Central for supplementary material.

Acknowledgments

We thank Dr. Lei Bruschweiler-Li and Dr. Huban Kutay for expert technical assistance. We thank The Ohio State University Comprehensive Cancer Center and Comparative Pathology for pathologic analysis. The NMR experiments were performed at The OSU CCIC NMR facility.

Financial Support: This work was supported, in part, by grants R01CA086978 (S. T. Jacob and K. Ghoshal) and R01CA193244 (K. Ghoshal) from the National Cancer Institute, a Pelotonia idea grant (S. T. Jacob) and a Pelotonia graduate fellowship (K.Y. Teng).

List of Abbreviations

mTOR	mechanistic target of rapamycin
STAT3	Signal transducer and activator of transcription 3
7-AAD	7-Aminoactinomycin D
PPP	Pentose phosphate pathway
TCA cycle	Tricarboxylic acid cycle
NMR	Nuclear magnetic resonance
HSQC	Heteronuclear single quantum coherence
TOCSY	Total correlation spectroscopy
G6P	Glucose-6-phosphate
F6P	Fructose-6-phosphate

GA3P	Glyceraldehyde-3-phosphate
GR3P	Glycerol-3-phosphate
3PG	3-Phosphoglyceric acid
GlcN	Glucosamine
GlcNAc	N-acetylglucosamine
DHAP	Dihydroxyacetone phosphate
Neu5Ac	N-acetylneuraminic acid
2-KG	α-ketoglutaric acid
Glu	Glutamic acid
Gln	Glutamine
Asp	Aspartic acid
DSS	4,4-dimethyl-4-silapentane-1-sulfonic acid

References

1. Llovet JM, Zucman-Rossi J, Pikarsky E, et al. Hepatocellular carcinoma. Nat Rev Dis Primers. 2016; 2:16018. [PubMed: 27158749]
2. Singal AG, El-Serag HB. Hepatocellular Carcinoma From Epidemiology to Prevention: Translating Knowledge into Practice. Clin Gastroenterol Hepatol. 2015; 13:2140–2151. [PubMed: 26284591]
3. Pusapati RV, Daemen A, Wilson C, et al. mTORC1-Dependent Metabolic Reprogramming Underlies Escape from Glycolysis Addiction in Cancer Cells. Cancer Cell. 2016; 29:548–562. [PubMed: 27052953]
4. Patra KC, Wang Q, Bhaskar PT, et al. Hexokinase 2 is required for tumor initiation and maintenance and its systemic deletion is therapeutic in mouse models of cancer. Cancer Cell. 2013; 24:213–228. [PubMed: 23911236]
5. Martinez-Outschoorn UE, Peiris-Pages M, Pestell RG, Sotgia F, Lisanti MP. Cancer metabolism: a therapeutic perspective. Nat Rev Clin Oncol. 2017; 14:113.
6. Prasannan R, Kalesh KA, Shanmugam MK, et al. Key cell signaling pathways modulated by zerumbone: role in the prevention and treatment of cancer. Biochem Pharmacol. 2012; 84:1268–1276. [PubMed: 22842489]
7. Casey SC, Amedei A, Aquilano K, et al. Cancer prevention and therapy through the modulation of the tumor microenvironment. Semin Cancer Biol. 2015; 35(Suppl):S199–223. [PubMed: 25865775]
8. Tzeng TF, Liou SS, Chang CJ, Liu IM. Zerumbone, a Natural Cyclic Sesquiterpene of Zingiber zerumbet Smith, Attenuates Nonalcoholic Fatty Liver Disease in Hamsters Fed on High-Fat Diet. Evid Based Complement Alternat Med. 2013; 2013:303061. [PubMed: 24223615]
9. Rahman HS, Rasedee A, Yeap SK, et al. Biomedical properties of a natural dietary plant metabolite, zerumbone, in cancer therapy and chemoprevention trials. Biomed Res Int. 2014; 2014:920742. [PubMed: 25025076]
10. Reyes R, Wani NA, Ghoshal K, Jacob ST, Motiwala T. Sorafenib and 2-Deoxyglucose Synergistically Inhibit Proliferation of Both Sorafenib-Sensitive and -Resistant HCC Cells by Inhibiting ATP Production. Gene Expr. 2017; 17:129–140. [PubMed: 27938509]
11. Lewis IA, Karsten RH, Norton ME, Tonelli M, Westler WM, Markley JL. NMR method for measuring carbon-13 isotopic enrichment of metabolites in complex solutions. Anal Chem. 2010; 82:4558–4563. [PubMed: 20459129]

12. Bingol K, Li DW, Zhang B, Brüschweiler R. Comprehensive Metabolite Identification Strategy Using Multiple Two-Dimensional NMR Spectra of a Complex Mixture Implemented in the COLMARm Web Server. Anal Chem. 2016; 88:12411–12418. [PubMed: 28193069]
13. Teng KY, Han J, Zhang X, et al. Blocking the CCL2-CCR2 Axis Using CCL2-Neutralizing Antibody Is an Effective Therapy for Hepatocellular Cancer in a Mouse Model. Mol Cancer Ther. 2017; 16:312–322. [PubMed: 27980102]
14. Takubo K, Nagamatsu G, Kobayashi CI, et al. Regulation of glycolysis by Pdk functions as a metabolic checkpoint for cell cycle quiescence in hematopoietic stem cells. Cell Stem Cell. 2013; 12:49–61. [PubMed: 23290136]
15. Lee IH, Finkel T. Metabolic regulation of the cell cycle. Curr Opin Cell Biol. 2013; 25:724–729. [PubMed: 23890700]
16. Lien EC, Lyssiotis CA, Cantley LC. Metabolic Reprogramming by the PI3K-Akt-mTOR Pathway in Cancer. Recent Results Cancer Res. 2016; 207:39–72. [PubMed: 27557534]
17. Yang JD, Roberts LR. Hepatocellular carcinoma: A global view. Nat Rev Gastroenterol Hepatol. 2010; 7:448–458. [PubMed: 20628345]
18. Singh S, Singh PP, Roberts LR, Sanchez W. Chemopreventive strategies in hepatocellular carcinoma. Nat Rev Gastroenterol Hepatol. 2014; 11:45–54. [PubMed: 23938452]
19. Wang B, Hsu SH, Frankel W, Ghoshal K, Jacob ST. Stat3-mediated activation of microRNA-23a suppresses gluconeogenesis in hepatocellular carcinoma by down-regulating glucose-6-phosphatase and peroxisome proliferator-activated receptor gamma, coactivator 1 alpha. Hepatology. 2012; 56:186–197. [PubMed: 22318941]
20. Wang B, Majumder S, Nuovo G, et al. Role of microRNA-155 at early stages of hepatocarcinogenesis induced by choline-deficient and amino acid-defined diet in C57BL/6 mice. Hepatology. 2009; 50:1152–1161. [PubMed: 19711427]
21. Ghoshal K, Li X, Datta J, et al. A folate- and methyl-deficient diet alters the expression of DNA methyltransferases and methyl CpG binding proteins involved in epigenetic gene silencing in livers of F344 rats. J Nutr. 2006; 136:1522–1527. [PubMed: 16702315]
22. Kutay H, Bai S, Datta J, et al. Downregulation of miR-122 in the rodent and human hepatocellular carcinomas. J Cell Biochem. 2006; 99:671–678. [PubMed: 16924677]
23. Llovet JM, Villanueva A, Lachenmayer A, Finn RS. Advances in targeted therapies for hepatocellular carcinoma in the genomic era. Nat Rev Clin Oncol. 2015; 12:436.
24. Dhanasekaran R, Bandoh S, Roberts LR. Molecular pathogenesis of hepatocellular carcinoma and impact of therapeutic advances. F1000Res. 2016; 5
25. Reyes RK, Motiwala T, Jacob ST. Regulation of glucose metabolism in hepatocarcinogenesis by microRNAs. Gene Expr. 2014; 16:85–92. [PubMed: 24801169]
26. Tsutsumi S, Fukasawa T, Yamauchi H, et al. Phosphoglucose isomerase enhances colorectal cancer metastasis. Int J Oncol. 2009; 35:1117–1121. [PubMed: 19787266]
27. Ahmad A, Aboukameel A, Kong D, et al. Phosphoglucose isomerase/autocrine motility factor mediates epithelial-mesenchymal transition regulated by miR-200 in breast cancer cells. Cancer Res. 2011; 71:3400–3409. [PubMed: 21389093]
28. Lyu Z, Chen Y, Guo X, et al. Genetic variants in glucose-6-phosphate isomerase gene as prognosis predictors in hepatocellular carcinoma. Clin Res Hepatol Gastroenterol. 2016; 40:698–704. [PubMed: 27288297]
29. Hay N. Reprogramming glucose metabolism in cancer: can it be exploited for cancer therapy? Nat Rev Cancer. 2016; 16:635–649. [PubMed: 27634447]
30. Zhao Y, Butler EB, Tan M. Targeting cellular metabolism to improve cancer therapeutics. Cell Death Dis. 2013; 4:e532. [PubMed: 23470539]
31. Cho RJ, Campbell MJ, Winzeler EA, et al. A genome-wide transcriptional analysis of the mitotic cell cycle. Mol Cell. 1998; 2:65–73. [PubMed: 9702192]
32. Tyagi AK, Singh RP, Agarwal C, Chan DC, Agarwal R. Silibinin strongly synergizes human prostate carcinoma DU145 cells to doxorubicin-induced growth Inhibition, G2-M arrest, and apoptosis. Clin Cancer Res. 2002; 8:3512–3519. [PubMed: 12429642]

Implications

Dietary compounds, like zerumbone, that impact cell cycle, apoptotic, and metabolic processes may have therapeutic benefits for HCC patients.

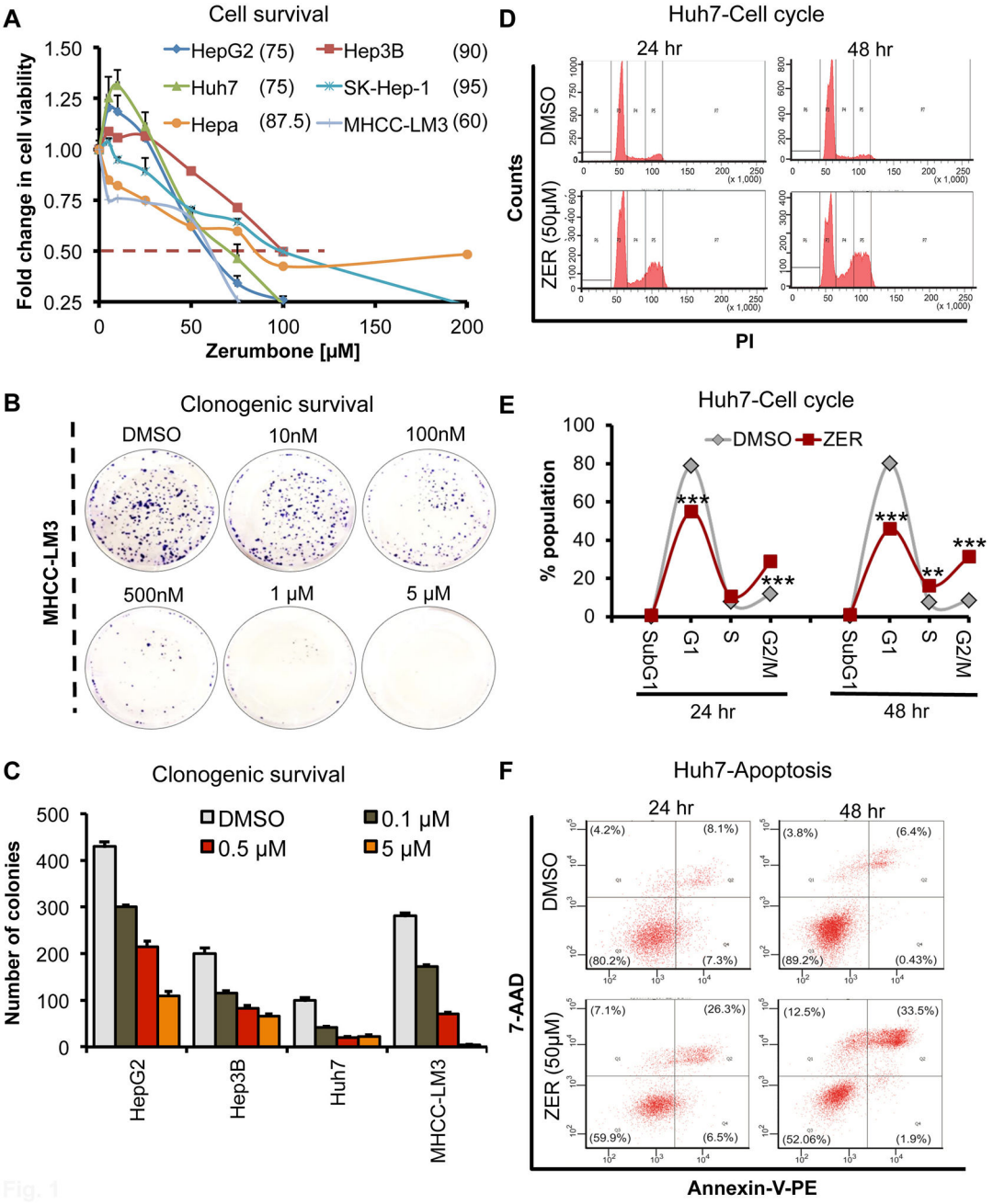

Fig. 1. Zerumbone (ZER) inhibits tumorigenic properties of HCC cells *in vitro*

(A) Dose response curve of HCC cell lines treated with ZER for 48 hours. Cells proliferation was measured by Cell Titer GLO assay. The average value in DMSO treated cells was arbitrarily assigned as 1. Error bars represent the standard deviation of biological triplicates. (**B, C)** Clonogenic survival of MHCC-LM3 cells after ZER treatment for 3 weeks. Colonies stained with crystal violet were imaged **(B)** and counted using ImageJ **(C)**. (**D, E)** Cell cycle profile of Huh7 cells treated with ZER (50 μM) for 24 and 48 hours as determined by flow cytometric analysis after propidium iodide staining. Cells at different stages of cell cycle were quantified by FlowJo software. (**F)** Population of Huh7 cells

undergoing apoptosis following ZER (50 μM) treatment as determined by flow cytometry following Annexin V/7-AAD staining. Values in parenthesis represent % of cells at each apoptotic stage. *p<0.05, **p<0.01 and ***p<0.001, two tailed t-test

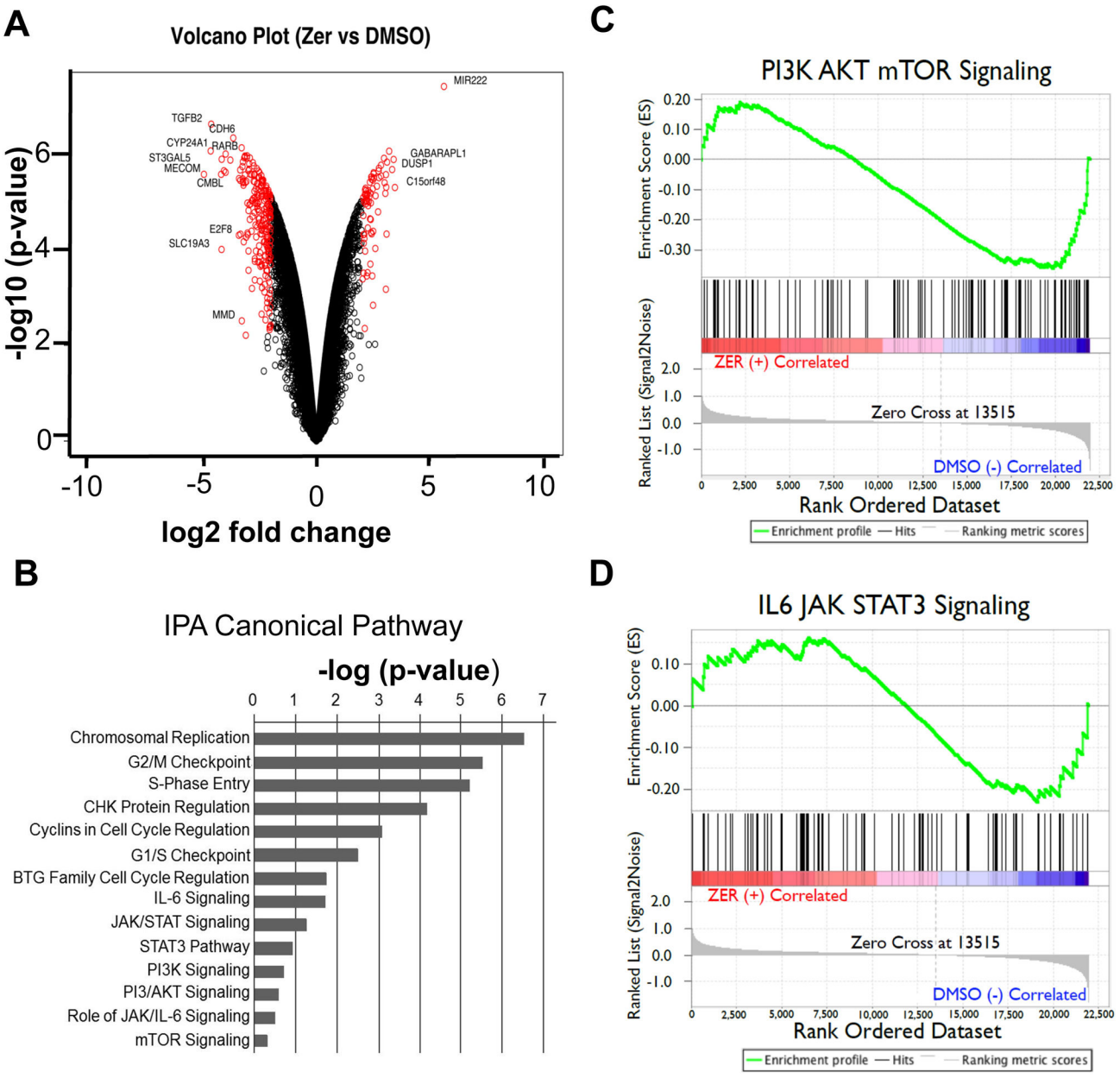

Fig. 2. ZER modulates expression of genes regulated by PI3/AKT/mTOR- and STAT3 - signaling in HCC cells

(A) Volcano plot of microarray data representing genes deregulated in MHCC-LM3 cells treated with ZER (50 μM) for 24 hours. **(B)** Enrichment of canonical pathways classified according to $-\log_{10}$(p-value) generated by IPA for genes altered by ZER treatment in MHCC-LM3 cells. **(C, D)** Gene set enrichment of PI3/AKT/mTOR- and STAT3 - signaling pathways in MHCC-LM3 cells treated with ZER.

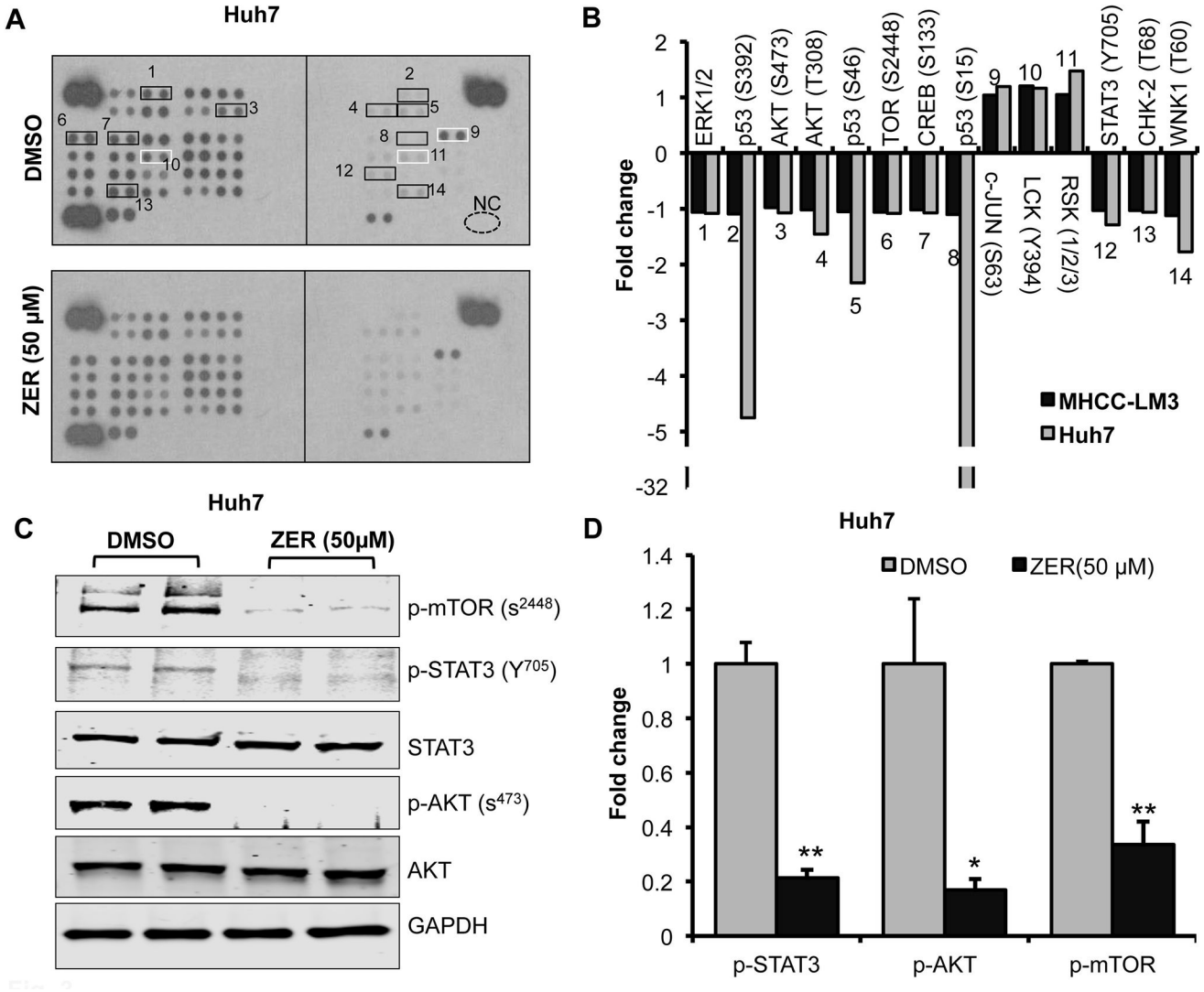

Fig. 3. ZER alters phosphoprotein profiles including that of AKT/mTOR and STAT3 in HCC cells

(A) Phosphokinase profiling in Huh7 cells treated with ZER. Lysates (250μg protein) from cells treated with ZER (50 μM) or DMSO for 24 hours were analyzed for relative levels of phosphorylation of 43 protein phosphorylation sites using antibody array kits. Black and white boxes mark the hypo- and hyper- phosphorylated proteins, respectively. (**B)** Quantitative analysis of altered phosphorylation in ZER treated Huh7 and MHCC-LM3 cells. Quantitation was done using Image J. (**C)** Immunoblotting of several kinases in Huh7 cells treated with ZER (50 μM) for 24 hours. (**D)** Quantitative analysis of phosphoproteins altered in Huh7 cells treated with ZER. *p<0.05 and **p<0.01, two tailed t-test

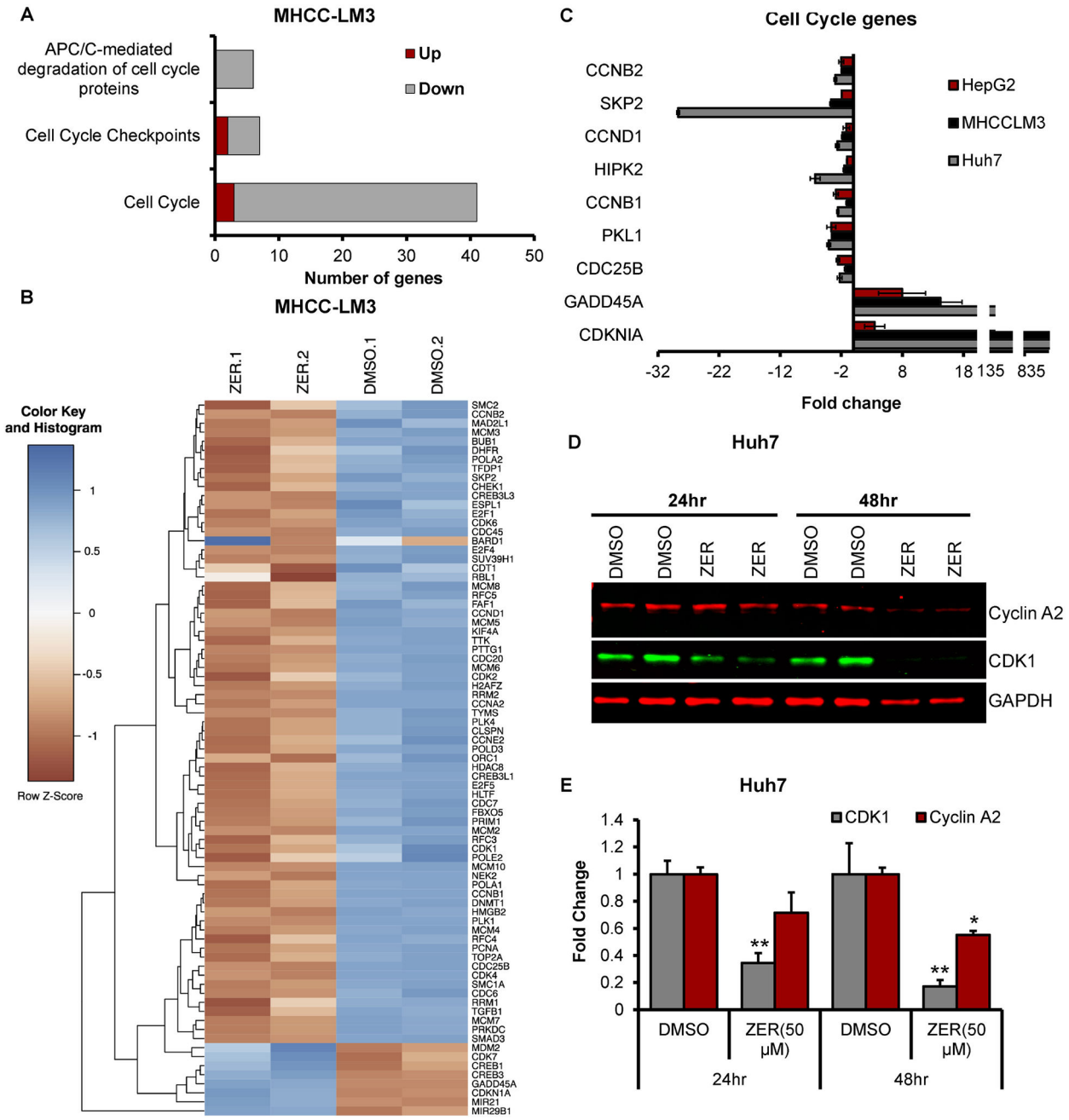

Fig. 4. ZER regulates expression of genes involved in cell cycle

(A) Altered expression of genes associated with cell cycle in MHCC-LM3 cells treated with ZER for 24 hours identified by microarray analysis. (**B)** Heatmap of ZER deregulated genes associated with cell cycle in MHCC-LM3 cells. (**C)** qRT-PCR analysis of cell cycle genes in indicated HCC cells treated with ZER. **(D)** Western blot analysis of proteins regulating G2 phase of cell cycle in Huh7 cells treated with ZER. (**E)** Quantitative analysis of proteins altered in Huh7 cells treated with ZER. *p<0.05, **p<0.01 and ***p<0.001, two tailed t-test

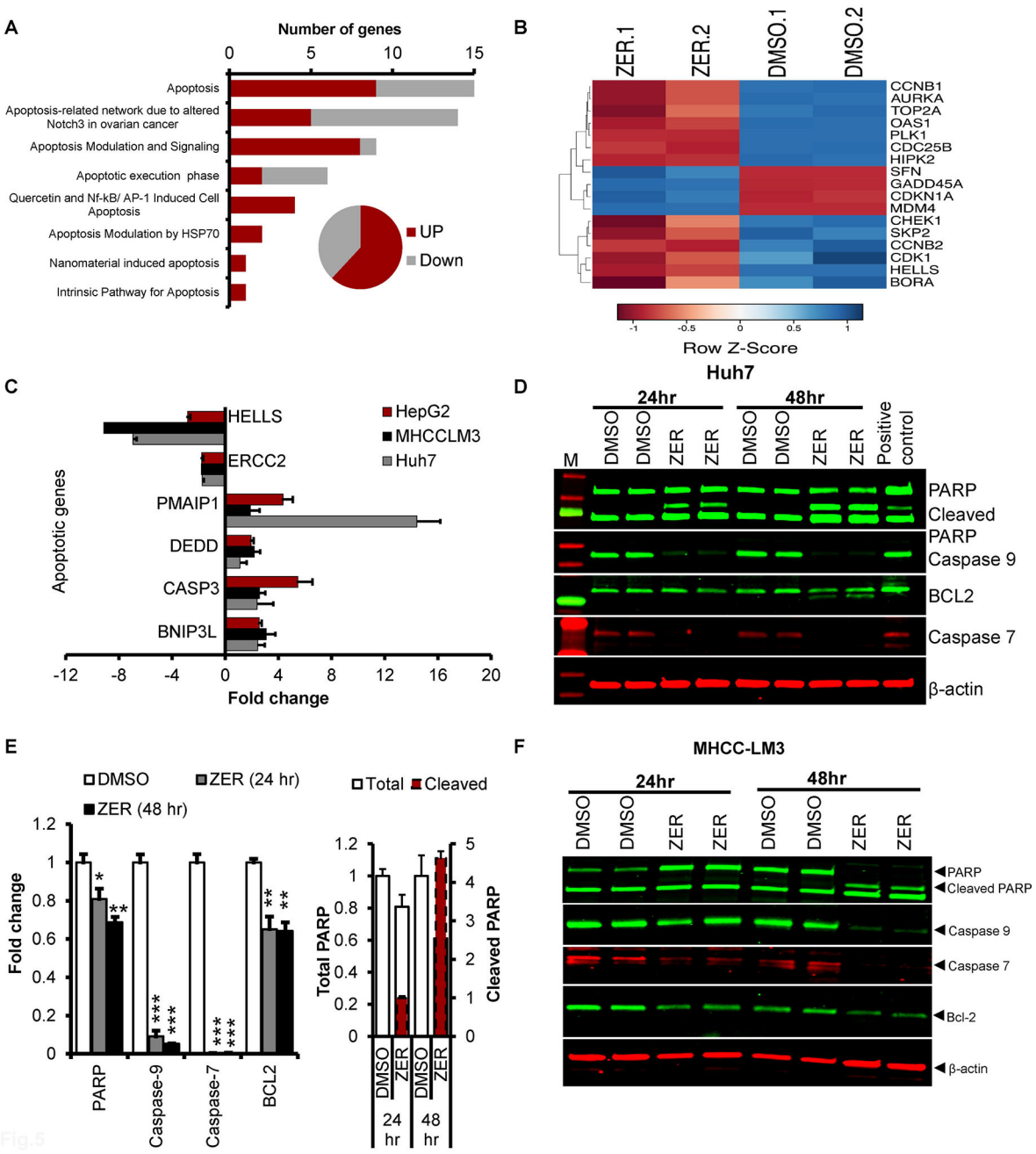

Fig. 5. ZER regulates expression of genes involved in apoptosis

(A) Altered expression of genes associated with apoptosis in MHCC-LM3 cells treated with ZER for 24 hours. (**B)** Heatmap of ZER deregulated genes associated with apoptosis in MHCC-LM3 cells. (**C)** qRT-PCR analysis of several pro- and anti- apoptotic genes in indicated HCC cell lines treated with ZER. (**D)** Western blot analysis of indicated proteins in Huh7 cells treated with ZER. (**E)** Quantitation of the western data. **(F)** Immunoblotting of indicated proteins in MHCC-LM3 cells treated with ZER. *p<0.05, **p<0.01 and ***p<0.001, two tailed t-test

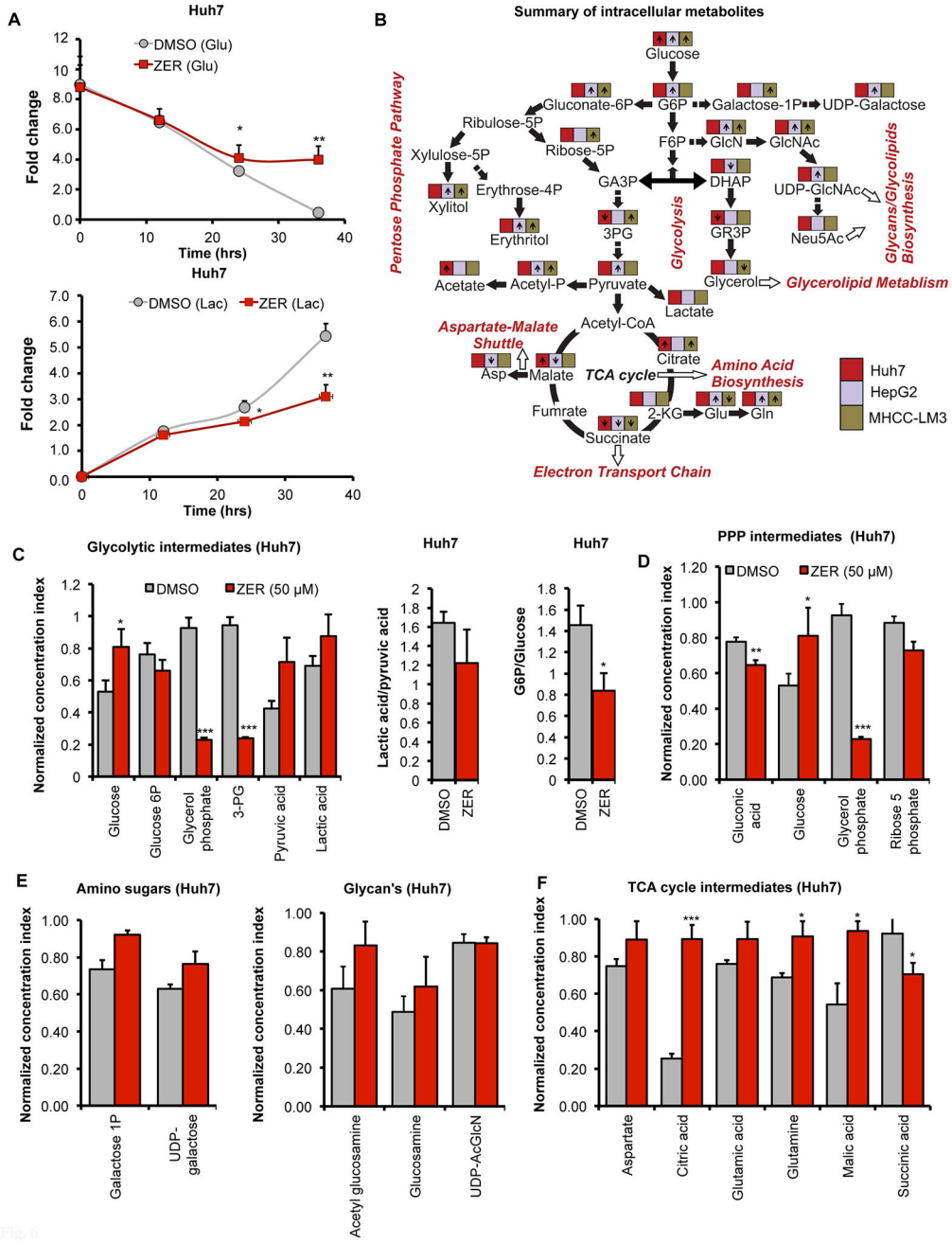

Fig. 6. ZER regulates glucose metabolism in HCC cells

(A) Glucose (upper panel) and lactate (lower panel) levels in culture supernatants from Huh7 cells treated with ZER/DMSO for indicated time points as measured by 2D ^{13}C-edited ^{1}H-^{1}H TOCSY NMR. (**B)** Summary of the alteration in levels of intracellular metabolites measured by 2D ^{13}C-^{1}H NMR in indicated HCC cell lines following ZER treatment. (**C)** Normalized concentration index of glycolytic intermediates and ratio of G6P to glucose and lactate to pyruvate levels in Huh7 cells treated with ZER or DMSO for 24 hours, **(D)** PPP metabolites, **(E)** galactose-1-P and UDP-galactose, amino sugars, and **(F)** TCA cycle

intermediates extracted from Huh7 cells treated with ZER or DMSO for 24 hours. *p<0.05, **p<0.01 and ***p<0.001, two tailed t-test

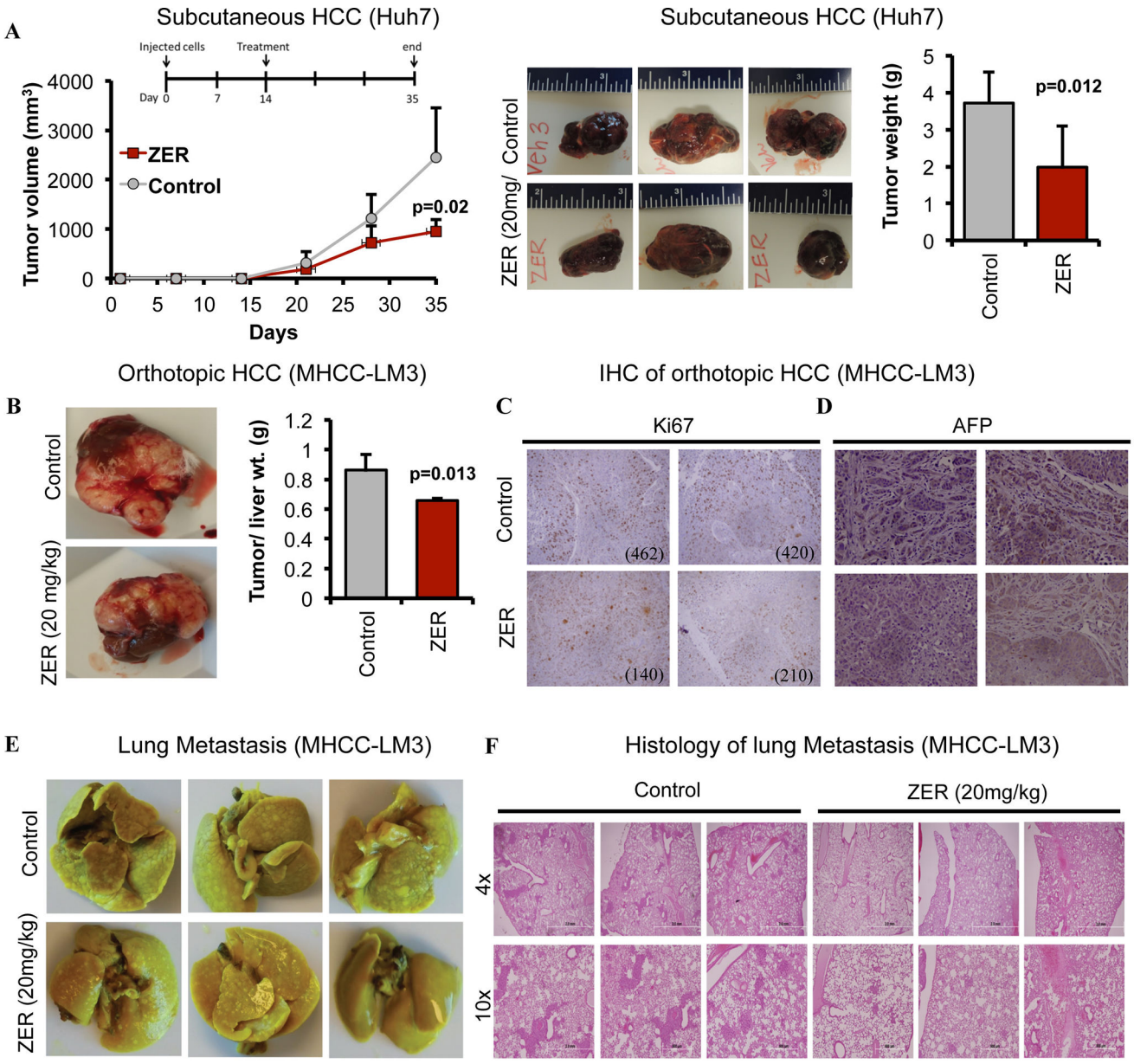

Fig. 7. ZER reduces HCC tumor growth and lung metastasis

(**A)** NSG mice bearing subcutaneous Huh7 xenografts were injected (I.P.) with ZER (20 mg/kg/day) or vehicle for 3 weeks. Tumor volume during treatment, representative pictures of tumors and average tumor weights at the end of experiment are provided. (**B)** NSG mice bearing orthotopic MHCC-LM3 xenografts were treated with ZER for 3 weeks. Representative pictures of the tumors and ratio of tumor weight to liver weight of mice are shown. **(C)** Ki-67- and (**D)** AFP- stained tumor sections in vehicle (HPBCD) or ZER treated mice. The numbers of Ki-67 positive cells at 20X magnification are provided within each picture. (**E)** Metastatic lung tumors developed in NSG mice bearing orthotopic MHCC-LM3 xenografts treated with vehicle or ZER for 3 weeks, and **(F)** H&E stained lung sections showing metastatic nodules.